Climate Dynamics manuscript No.
(will be inserted by the editor)

Stable AMOC off state in an eddy-permitting Coupled Climate Model

J.V. Mecking · S.S. Drijfhout · L.C. Jackson · T. Graham

Received: date / Accepted: date

J.V. Mecking
Ocean and Earth Science
National Oceanography Centre Southampton
University of Southampton
UK, SO14 3ZH
Tel.: +44 2380 59 4064
E-mail: j.mecking@noc.soton.ac.uk

S.S. Drijfhout
Ocean and Earth Science
National Oceanography Centre Southampton
University of Southampton
UK, SO14 3ZH

L.C. Jackson
Met Office
Hadley Centre
Fitzroy Road

Abstract Shifts between on and off states of the Atlantic Meridional Overturning Circulation (AMOC) have been associated with past abrupt climate change, supported by the bistability of the AMOC found in many older, coarser resolution, ocean and climate models. However, as coupled climate models evolved in complexity a stable AMOC off state no longer seemed supported. Here we show that a current-generation, eddy-permitting climate model has an AMOC off state that remains stable for the 450-year duration of the model integration. Ocean eddies modify the overall freshwater balance, allowing for stronger northward salt transport by the AMOC compared with previous, non eddy-permitting models. As a result, the salinification of the subtropical North Atlantic, due to a southward shift of the intertropical rain belt, is counteracted by the reduced salt transport of the collapsed AMOC. The reduced salinification of the subtropical North Atlantic allows for an anomalous northward freshwater transport into the subpolar North Atlantic dominated by the gyre component. Combining the anomalous northward freshwater transport with

Exeter UK, EX1 3PB

T. Graham
Met Office
Hadley Centre
Fitzroy Road
Exeter UK, EX1 3PB

the freshening due to reduced evaporation in this region helps stabilise the AMOC off state.

Keywords AMOC · AMOC collapse · abrupt climate change · hosing experiment · CGCM · eddy-permitting

1 Introduction

The Atlantic Meridional Overturning Circulation (AMOC) describes the meridional volume transport in the Atlantic Ocean (Wunsch, 2002). The AMOC brings warm waters to the high latitude North Atlantic, warming the climate of Northern and Western Europe. A collapse of the AMOC would lead to drastic changes in surface air temperatures over much of the Northern Hemisphere, in particular in the Northeast Atlantic where temperatures can drop by 9°C (Manabe and Stouffer, 1988; Vellinga and Wood, 2002; Jackson et al, 2015). As a consequence of anthropogenic climate change, warming of the high latitude North Atlantic and the addition of freshwater through enhanced precipitation, increased melting of sea-ice and icebergs, as well as more runoff from the Greenland ice sheet can cause the sinking branch of the AMOC to weaken and potentially shut down. Hereafter, we refer to a collapsed AMOC as an AMOC off state while, the AMOC circulation, as it is known today, is referred to as an AMOC on state.

Climate model projections indicate a likely weakening of the AMOC, but a complete collapse was deemed unlikely in the latest IPCC report by Collins et al (2013). However, models have difficulty correctly simulating past abrupt climate changes, including an AMOC collapse, affecting the likelihood of simulating future abrupt climate change (Valdes, 2011; Drijfhout et al, 2011). Paleo-proxy data have shown evidence for wide spread abrupt climate change events in the times before the Holocene from ice-core records (Dansgaard et al, 1993; Blunier and Brook, 2001) and sediment cores (de Abreu et al, 2003). A possible interpretation of these events is that they are associated with switches between AMOC on and off states in the past (Broecker et al, 1990), although the spatial extent of these abrupt changes in climate can still be questioned (Wunsch, 2006). Such switches can be theoretically understood from simple box model studies showing that under the same forcing conditions it is possible to have both a stable AMOC on and off state, or only a mono-stable regime depending on the forcing (Stommel, 1961; Marotzke, 1990; Rahmstorf, 1996). The existence of bistability in these box models depends on the freshwater forcing. Similarly, some coupled climate models have found a bistable AMOC dependent on freshwater forcing when freshwater hosing was applied continuously (Hawkins et al, 2011; Hu et al, 2012; Sijp, 2012). However, in newer coupled climate models after applying freshwater hosing for a set amount of time the AMOC recovered after the freshwater hosing was stopped (Peltier et al, 2006; Krebs and Timmermann, 2007; Jackson, 2013) while it was possible to maintain the AMOC off state in some older coupled climate models (e.g. UVic and GFDL R30 models in Stouffer et al (2006)).

To identify the transition between the two regimes of mono- and bistability it was proposed that the sign of the freshwater transport by the AMOC in the

Atlantic can be used as an indicator for its stability (referred to here as M_{ov} but often also referred to as F_{ov}) (Rahmstorf, 1996; de Vries and Weber, 2005). When used as an indicator for AMOC stability, M_{ov} is typically measured at the southern entrance of the Atlantic near 34°S. A positive M_{ov} at 34°S indicates that the AMOC imports freshwater into the Atlantic and a negative M_{ov} at 34°S indicates freshwater export from the Atlantic. In an AMOC off state M_{ov} is expected to tend towards zero, thereby creating an anomalous salt import into the Atlantic for positive M_{ov} which leads to a destabilisation of the AMOC off state. On the other hand, when M_{ov} is negative an AMOC collapse will result in an anomalous freshwater import into the Atlantic helping stabilise the AMOC off state. Therefore, a positive M_{ov} can be associated with a mono-stable AMOC while a negative M_{ov} can be associated with a bistable AMOC (Huisman et al, 2010). Observational estimates of M_{ov} at the southern boundary of the Atlantic based on ship data or estimated from ARGO float data support a negative M_{ov}, suggesting that the present day AMOC resides in the bistable regime (Bryden et al, 2011; Garzoli et al, 2013). It has been recommended that the divergence of the freshwater transport into the Atlantic by the AMOC, $\Delta M_{ov} = M_{ovS} - M_{ovN}$, where S (N) is the southern (northern) boundary of the Atlantic is a better indicator of bistability (Huisman et al, 2010; Liu and Liu, 2013).

When the AMOC weakens and even collapses, the reduction in northward heat transport causes a wide spread cooling of the northern hemisphere surface air temperatures (Manabe and Stouffer, 1988; Vellinga and Wood, 2002; Jackson et al, 2015). The cooling leads to a southward/equatorward shift of the latitude of maximum heating causing the dividing latitude of the northern and southern hemisphere Hadley circulations to shift southward (Drijfhout, 2010), displacing the Intertropical Convergence Zone (ITCZ). The southward shift of the ITCZ causes a reduction of precipitation in the subtropical North Atlantic region leading to a salinification of the ocean. The saltier waters in this region can be transported into the high latitude regions of the North Atlantic through large-scale instabilities kick starting the convection (e.g. the large-scale eddy generated in GFDL CM2.1 in Yin and Stouffer (2007)). Therefore, in order for the AMOC off state to remain stable this salinification needs to be balanced by an equally large freshening term, due to changes in ocean circulation.

In the GFDL R30 model the freshening associated with ocean circulation changes is large enough to counteract the salinification due to the southward ITCZ shift because the overturning circulation reverses (Yin and Stouffer, 2007). In that case Antarctic Intermediate Water (AAIW) sinks to a depth of 1000 m just south of South America and is transported northward, then upwells in the North Atlantic subtropical gyre. This circulation has been named the reverse thermohaline circulation (RTHC). However, the RTHC only develops in coarse-resolution ocean models and often is deeper than just the upper 1000 m (Dijkstra, 2007; Hawkins et al, 2011; Sijp, 2012). In a newer generation of coupled climate models the RTHC cell does not develop (e.g. GFDL CM2.1 in Yin and Stouffer (2007)) and without the additional freshwater transport of the RTHC the subtropical gyre becomes so salty that a fresh subpolar ocean without deep sinking is no longer stable and the AMOC recovers (Yin and Stouffer, 2007; Jackson, 2013). The reason for the RTHC not to develop is that stronger atmospheric feedbacks promote saltier and colder thermocline water in the subtropical North Atlantic, reducing the north-south pressure gradient between the subtropical North Atlantic and subpolar South Atlantic that is driving the RTHC (Yin and Stouffer, 2007)).

In the very latest coupled climate models ocean eddies and swifter boundary currents are allowed for, changing the salt balance in the Atlantic. Ocean eddies freshen the subtropical gyre by exchanging water with the tropics and subpolar gyre (Tréguier et al, 2012). As a result, eddy-permitting and eddy-resolving models must feature a larger mean flow salt transport divergence into the subtropical gyre to maintain equilibrium counteracting freshening by the eddies. The larger mean flow salt transport divergence could allow for a stronger advective salt feedback associated with an AMOC collapse without the need of developing an RTHC. Indeed, using a higher resolution coupled climate model Spence et al (2013) achieved a stronger drop and slower recovery of the AMOC in a high-resolution model relative to a coarser resolution model in a relatively weak and short freshwater hosing experiment. Similarly, Weijer et al (2012), using an ocean only model, were able to show that the drop in AMOC in response to a freshwater hosing was stronger in the higher resolution model. Both studies suggest that the AMOC off state in higher resolution models could become stable. Here we discuss whether a larger salt transport by the AMOC into the North Atlantic subtropical gyre, which is typical for higher resolution ocean models, can sustain a stable off state, even if the RTHC does not develop, using a 450 year long hosing experiment in an eddy-permitting coupled climate model.

2 Model Configuration and Experiment Setup

2.1 Model Configuration

For this study the Global Climate version 2 (GC2) (Williams et al, 2015) configuration of Hadley Centre Global Environmental Model version 3 (HadGEM3) (Hewitt et al, 2011) is used. This coupled climate model consists of an ocean, atmosphere, sea-ice and land-surface model coupled together with data exchanging between the atmosphere and ocean components every 3 hours. The ocean model component of GC2, HadGEM3 uses the Global Ocean version 5 (GO5) (Megann et al, 2013) of the ORCA025 configuration of the Nucleus for European Modelling of the Ocean (NEMO) (Madec, 2008) version 3.4. The ORCA025 grid uses a tri-polar structure with poles over Antarctica, Siberia and Canada and has a horizontal resolution of 0.25°, with the resolution decreasing when moving towards the poles so that the grid remains quasi-isotropic. The ocean model contains 75 vertical levels with thicknesses ranging from 1 m at the surface and increasing with depth up to 200 m in the bottom layer. The sea-ice model is the global sea ice version 6 (GSI6) configuration of the Los Alamos National Laboratory sea ice model (CICE) version 3.4 (Rae et al, 2015) and is used at the same model grid as the ocean model. The Global Atmosphere version 6 (GA6.0) of the Met Office unified model is used with a horizontal resolution of N216, which has a resolution of about 60 km in mid-latitudes, and has 85 levels in the vertical leading to an improved resolution in the stratosphere. Global Land version 6 (GL6) configuration of the land model Joint UK Land Environment Simulator (JULES) is also used in this model setup but none of its data is analysed in this study. Heat, freshwater and momentum fluxes are passed between the atmosphere and ocean/ice model every three hours through the OASIS coupler while the ocean and sea-ice model exchange fluxes every ocean model time step (22.5 min) without the use of flux adjustment. The eddy permitting resolution of the ocean model has lead to a reduction in the North Atlantic cold bias and the atmospheric model shows improved Atlantic and European blocking events (Scaife et al, 2011) and the ability to better predict the winter North Atlantic Oscillation (Scaife et al, 2014), in previous versions of the HadGEM3 model setup, i.e. GloSea5.

2.2 Experiment Setup

In this study two experiments from the GC2 model are considered, a 150-year long present day control simulation and a 450 year long hosing experiment. The hosing experiment is a continuation of the experiment analysed in Jackson et al (2015) (See reference for more details). The present day control simulation was started from a 36 year long development run of HadGEM3, which was initialised with EN3 data (Ingleby and Huddleston, 2007) averaged over

2004-2008 and the hosing experiment is started from year 42 of the control experiment. The control simulation uses CO2 concentrations based on 1978 levels and held constant throughout both simulations. The main goal of the hosing experiment was to collapse the AMOC, therefore, the methodology is based on Vellinga and Wood (2002), which allows for a rapid collapse of the AMOC but is very idealised. For the first 10 years of the hosing experiment the salinity in the model is perturbed by an amount equivalent to a hosing of 10 Sv, making a total of 100 Sv·years additional freshwater. This is done through reducing the salinity in the Atlantic Ocean north of 20°N and in the Arctic by 0.64 psu in the upper 350 m and then tapering to zero over the next 186 m (Fig. 1). This is done instantaneously every December 1 and, as is common practice in hosing experiments, is compensated by adding 0.008 psu everywhere else in the ocean allowing for the total salinity to be conserved (Fig. 1). After the 10 years of hosing is completed and the model is allowed to continue without changes for another 440 years.

3 Results

In the 450 year long hosing experiment the AMOC is able to collapse and remain very weak for the entire duration of the model integration (Fig. 2). During and after the 10 year hosing period the ocean begins to adjust, with salinity anomalies slowly spreading southward from the hosing region towards the equator and also spreading downward in the water column. Since we want to discuss the evolution of the ocean fields in 100 year time-slices, we will take the period 311-410 (301 to 400 years after the hosing stopped) as representative for the final state of the model. The mean salinity is 0.86 psu fresher in the hosing region towards the end of the hosing simulation (years 311-410) relative to the control simulation. The sea surface salinity (SSS) anomaly with respect to the control run features a comma shaped pattern in the North Atlantic subtropical gyre (Fig. 3a), as typical with most fresh water hosing experiments (Krebs and Timmermann, 2007; Yin and Stouffer, 2007). The sea surface temperatures (SSTs) also drop due to the reduction of northward heat transport from the AMOC off state (Fig. 3b and Jackson et al (2015)). The decrease in SSTs allow for the seasonal sea-ice to extend further southward reaching as far south in winter as the Grand Banks, as well as covering a large portion of the Norwegian and Baltic Seas (Fig. 3b). The reductions in SSS and SST fall within the range of what has been seen in previous modelling studies with a similar magnitude of freshwater hosing (Yin and Stouffer, 2007).

3.1 AMOC Streamfunction

The control simulation features a realistic AMOC with a maximum strength of 17.4 Sv at 27°N and at a depth of 773 m in the mean (Fig. 4a). The depth reached by the North Atlantic Deep Water cell is slightly shallower than that in observations (3000 m as opposed to 4000 m in (Kanzow et al, 2010; Smeed et al, 2014)), a common problem in ocean models (Danabasoglu et al, 2014). The Faroe Bank Channel overflow (defined as waters denser than $\sigma_\theta = 27.8\ kg/m^3$) is slightly weaker in this model than in observations (1.8 Sv as opposed to 1.9

Sv (Hansen and Østerhus, 2007)). This overflow is mainly missing the weak cold waters below 0 °C which account for the majority of the overflow waters in the observations, making the model overflow less dense. For the Denmark Strait the overflows are considerably weaker when considering waters denser than $\sigma_\theta = 27.8\ kg/m^3$ (1.4 Sv as opposed to 3.4 Sv (Jochumsen et al, 2012)), which again is missing the very cold water masses. However, for the Denmark Strait choosing the density cut off to be $\sigma_\theta = 27.8\ kg/m^3$ misses a lot of the overflow waters. By choosing the density class cut off of to be $\sigma_\theta = 27.6\ kg/m^3$, matching the depth of density cutoff in Jochumsen et al (2012), the overflow increases to 2.9 Sv. These differences in the overflows between the model and observations could potentially lead to the shallower North Atlantic Deep Water cell. The main convection sites are in the Labrador Sea, Greenland Sea and South of Iceland (Fig. 4b) as expected from observations (de Boyer Montégut et al, 2004). However, the too buoyant overflows could potentially account for the slightly weaker and shallower AMOC as compared to observations at 26.5°N (Fig. 2a, 15.7 Sv as opposed to 17.5 Sv (Smeed et al, 2014)) but this is not investigated in more detail.

Based on an AMOC index at 26.5°N and between 500-2000 m the AMOC collapses very rapidly during the hosing, leading to a minimum in AMOC at year 4 (Fig. 2a). After the hosing has stopped the AMOC recovers slightly, achieving a maximum at year 21, before dropping in strength again and remaining in a very weak state for the duration of the model integration. However, there is a noticeable weak trend in the AMOC index at 26.5°N which by the end of the model integration causes the AMOC to increase in strength to just over 5 Sv (Fig. 2a). This increase in AMOC strength is slow and occurs later in the model integration than seen in previous climate model studies (Vellinga and Wood, 2002; Stouffer et al, 2006; Jackson, 2013). Also, it only applies to a shallow, wind-driven, AMOC that does not extend further north than the subtropics. Considering an AMOC index further to the north (maximum between 50°N - 65°N and 500-2000 m depth) the AMOC collapse shows no hint of recovering (Fig. 2b). There is no sign of increasing mixed layer depth in the subpolar North Atlantic due to the onset of deep convection (Fig. 4d). Both subtropical and subpolar wind-driven cells are enhanced near the surface related to the positive North Atlantic Oscillation (NAO) that develops in response to the AMOC collapse (Jackson et al, 2015). The AMOC streamfunction does not develop a stable RTHC after the AMOC collapses. Despite this, the AMOC off state appears stable, at least for 450 years. In year 311-410 there appears to be no convection present in the high latitude regions (Fig. 4d) and similarly the overflows in the Denmark Strait and Faroe Banks Channel have completely collapsed to 0 with no signs of recovery.

3.2 Atmospheric Response

The southward shift of the ITCZ is reflected in the net precipitation (precipitation - evaporation + runoff, PER) and causes a reduction in the surface freshwater flux into the ocean just north of the equator and an increase south of the equator (Fig. 5a,b). These changes in PER reduce the amount of freshwater added to the subtropical North Atlantic with the majority of the reduction in precipitation occurring in the subtropical North Atlantic which loses 0.047 Sv in years 311-410 (Table 1, Fig. 5c). This reduction in PER is an atmospheric feedback to the AMOC collapse that acts to destabilise the AMOC off state by salinifying the North Atlantic.

Over the subpolar North Atlantic evaporation is reduced due to the increase in sea-ice cover blocking latent heat exchange and the decrease in atmospheric temperatures reducing the amount of atmospheric water vapour content (Table 1, Fig. 5b) (Drijfhout, 2014). Despite the reduction in evaporation being small relative to the precipitation changes in the subtropical regions, it is large enough to outweigh the reduction in precipitation over the subpolar Atlantic. The subsequent increase in PER causes an anomalous freshening of the sinking regions (Fig. 5d) with a magnitude of 0.042 Sv in the years 311-410 (Table 1). The rate at which the precipitation and evaporation anomalies change reduces as the model integration continues, especially for the evaporation. This subpolar freshening is an atmospheric feedback that stabilises the AMOC off state through freshening the North Atlantic. The salinification over the subtropical North Atlantic is marginally stronger than the freshening over the subpolar North Atlantic (Table 1). The salinification of the subtropical North Atlantic could eventually lead to more saline waters being transported in the subpolar North Atlantic as seen in the GFDL CM2.1 model (Yin and Stouffer, 2007). Nevertheless, the off state remains stable here, while it quickly destabilises in the GFDL CM2.1 model. It should be noted that the initial atmospheric response of precipitation and evaporation in HadGEM3 is similar to that in GFDL CM2.1. However, in the GFDL CM2.1 model the precipitation anomalies associated with a southward shift of the ITCZ are not maintained as the AMOC recovers, while here the anomaly continues to show the characteristic dipole pattern over the equator although the amplitude is slowly decreasing (Fig. 5c). This brings up the question which additional feedbacks are present in HadGEM3, stabilising the AMOC off state? To answer this question we analyse in detail the freshwater budget in the subtropical and subpolar North Atlantic.

3.3 Freshwater Budget

The freshwater budget analysis is based on an extension to the calculations detailed in Drijfhout et al (2011) (see appendix for details). The freshwater budget can be summarised as follows:

$$M_{trend} = \Delta M_{ov} + \Delta M_{az} + \Delta M_{eddy} + PER + M_{mix}, \tag{1}$$

where M_{trend} is the freshwater trend in the region of interest, $\Delta M_{ov/az/eddy}$ represents the divergence of the freshwater transport for the specific region, in our case the southern boundary minus the northern boundary, for the various components of the transport, PER is the precipitation minus evaporation plus runoffs over the specific region of interest and finally M_{mix} is the residual term of the budget, mainly comprised of mixing along the boundaries. In eqn. 1 the decomposition of mean flow transport divergence into an overturning

(M_{ov}) and gyre (M_{az}) component was motivated by the much stronger coupling between M_{ov} and AMOC than between M_{az} and AMOC at the southern boundary of the Atlantic, when they budget is applied to the Atlantic as a whole. Especially in the North Atlantic subpolar gyre this decomposition can be questioned. However, this framework can still be used to link area integrated changes in freshwater budget to changes in the AMOC, especially in the North Atlantic subtropics. It appears that changes in M_{ov} are first order in eqn. 1 and can be understood from the AMOC collapse as they are dominated from changes in the zonal mean velocity field. In addition it allows for comparison with observations where freshwater transports have been diagnosed using the same framework (McDonagh et al, 2010; Bryden et al, 2011; Garzoli et al, 2013; McDonagh et al, 2015-in press). When the model is in an equilibrium state the changes in PER are approximately balanced by changes in freshwater transport by overturning circulation (M_{ov}), azonal circulation (M_{az}) and eddies (M_{eddy}). We apply the freshwater budget analysis to the subtropical North Atlantic, defined as 10°N to 45°N, and to the subpolar North Atlantic, defined to be 45°N to 70°N. These boundaries were chosen to coincide with the boundaries of the subtropical and subpolar gyres, with the subpolar gyre region containing the main sinking regions of the North Atlantic. The region specific freshwater budget analyses are summarised in Table 1 and graphically in Fig. 6. The atmospheric contributions to the freshwater budget have already been discussed; below we discuss the freshwater transport terms as well as the freshwater budget as a whole.

3.3.1 Freshwater Transports

The AMOC off state is associated with changes in the freshwater transport terms that must be able to balance the changes in PER, especially in the subtropical North Atlantic, to prevent a salinification of the North Atlantic and hence a return to the AMOC on state. In the control simulation the freshwater transport due to the overturning, M_{ov}, is negative throughout the entire Atlantic Ocean, indicating that the AMOC is transporting freshwater southward/salt northward (Fig. 7). The negative M_{ov} at 34°S is consistent with observations (Bryden et al (2011),Garzoli et al (2013), McDonagh Personal Communications based on McDonagh and King (2005)), despite being slightly weaker, and is a possible indication for a bistable AMOC (Fig. 7). After the AMOC collapses the magnitude of M_{ov}, as expected, decreases and over time adjusts to a new equilibrium (Fig. 8a). The reduction in magnitude of M_{ov} can be attributed to the reduction in AMOC transport, with changes in salinity only having a small effect (Fig. 8b). These changes lead to an anomalous northward transport of freshwater south of 45°N in the Atlantic Ocean (Fig. 8b). Even more important, however, is the sign of the divergence of M_{ov} instead of the sign of M_{ov} itself, since it is the divergence that determines whether or not there will be a freshening or salinification in the region of interest. The subtropical North Atlantic has an increase of 0.132 Sv of freshwater due to the changes in the divergence of M_{ov} (Fig. 6c, Table 1). The associated increase in freshwater is twice the amount of freshwater required to balance the anomalous salinification caused by changes in PER (Table 1). Changes in the divergence of M_{az} and M_{eddy} need to enhance the salinification caused by PER and thereby balance the changes in divergence of M_{ov}.

The salinity decrease after the AMOC collapse is largest at the eastern side of the basin, which does not only hold for the surface (Fig. 3a) but, also at depth (not shown). This decrease in salinity is strongest over the southward branch of the subtropical gyre and northward branch of the subpolar gyre, near the eastern boundary, leading to changes in M_{az}. This results in a decrease in M_{az} in the subtropical gyre and an increase in M_{az} in the subpolar gyre, while changes at the gyre boundaries are small (e.g 10°N and 45°N) (Fig. 8c,d). Relative to the climate models in Yin and Stouffer (2007), which have a coarser resolution, HadGEM3 has larger amplitude in M_{az} divergence, also leading to larger changes in its divergence after the collapse. This is due to the increase in model resolution leading to stronger gyres (Tréguier et al, 2005; Spence et al, 2013) and less east-west difference in salinity bias (Yin and Stouffer (2007) their Fig. 1), likely due to the Gulf Stream separation being too far north in lower resolution models. The change in divergence of M_{az} for both the subtropical and subpolar North Atlantic reduces the amount of freshwater being transported into these regions (Fig. 6, Table 1). This anomaly in freshwater transport partially balances the additional freshwater being added to the subtropical North Atlantic by changes in M_{ov} (Table 1, Fig. 6c) and changes in the subpolar gyre PER and mixing (Fig. 6b).

The resolution of the model used in this study allows for the analysis of the effect of eddies on the freshwater budget from the equator to mid latitudes.

Here, freshwater transport due to eddies is defined as the difference between total freshwater transport and freshwater transport calculated by using the seasonal fields only (see appendix for more details). The main effect of the eddies is to exchange water between the subtropical and subpolar gyres, freshening the former and salinifying the latter (Fig. 8e and Table 1). Immediately after the AMOC collapse the salinity gradient at the edge of the hosing region becomes very large leading to a large increase in the southward freshwater transport by the eddies at 20°N. Within a few decades after the freshwater hosing M_{eddy} becomes relatively small again compared to M_{ov} and M_{az} with values similar to the control integration (Fig. 8e). In the eddy-permitting model the freshening of the subtropical North Atlantic by M_{eddy} and the increased freshening by a larger M_{az} play a similar role to the flux adjustment in coarser resolution climate models in the control integration (e.g. GFDL R30 model in Yin and Stouffer (2007)). This helps to stabilise the freshwater budget by allowing for a larger negative M_{ov} in the control integration and subsequently a larger change in M_{ov} after the AMOC collapses. The change in M_{ov} is now large enough to balance all other terms in the freshwater budget without leaving a strong positive salinity trend in the subtropical North Atlantic. As model resolution increases further towards eddy-resolving the magnitude of M_{eddy} is expected to become even larger (Tréguier et al, 2012), further adding to the stabilising effect of the eddies.

3.3.2 Total Freshwater Budget

The total freshwater trend in the subtropical North Atlantic still shows a small salinification over the 311-410 year period, slightly stronger than the salinification in the control run (Table 1, Fig. 6). Despite the salinification of the subtropical North Atlantic, the subpolar North Atlantic shows a freshening trend, enhancing the salinity gradient between the two (Table 1, Fig. 6). The anomalous freshening trend of the subpolar North Atlantic can be attributed to the combination of decreased evaporation in this region, the anomalous northward freshwater transport at the gyre boundaries and an increased mixing term (i.e M_{mix}). The gradient in salinity across the North Atlantic, despite being stronger than in the control integration, does not lead to large-scale instabilities that suddenly give rise to very strong salinity transports as seen in Yin and Stouffer (2007). The eddies are likely helping to keep the gradient small enough to avoid a sudden large-scale instability to develop and to restart the convection in the high latitude sinking regions.

4 Discussion

The AMOC response to freshwater perturbations has been previously investigated in a large CMIP/PMIP coordinated experiment (Stouffer et al, 2006). A freshwater hosing of 0.1 Sv and 1 Sv was applied for 100 years, versus a hosing of 10 Sv over 10 years in the present experiment. Of the nine models involved in the 100 Sv·year hosing experiment, seven models had started the transition from the off state back to the on state before 100 years after the completion of the hosing. Two models remained in the off state; one model of intermediate complexity, Uvic, and one older GFDL model, GFDL R30. The different behaviour between GFDL R30 and a newer version, GFDL CM2.1, was afterwards analysed (Yin and Stouffer, 2007) and it was argued that the stable off state in GFDL R30 was maintained by flux adjustment and weak atmospheric feedbacks allowing the RTHC to develop. This result led to the paradigm that newer generation climate models that no longer use flux adjustment and feature more realistic atmospheric dynamics are not able to maintain a stable AMOC off state (Yin and Stouffer, 2007; Liu et al, 2014). Here we show that an eddy-permitting coupled climate model is able to maintain a stable AMOC off state for 440 years after the hosing is completed, which is more than twice as long as the runs performed in the CMIP/PMIP experiment. The increase in freshwater transport into the subtropical North Atlantic due to higher-resolution eddies and increased boundary currents allow the AMOC to transport more salt northwards across the entire Atlantic basin. This stronger advective salt feedback is key for the model to be able to counteract the strong atmospheric response over the tropical/subtropical North Atlantic basin that features in complex climate models when the AMOC collapses. In a sense, eddies and swifter boundary currents play a similar role in the freshwater budget to the flux adjustment used in older generation climate models.

Some coupled climate models of lower complexity have been integrated for even longer durations with some of them having the AMOC off state become unstable after many centuries (Krebs and Timmermann, 2007). We cannot exclude that such a transition will eventually occur in HadGEM3, but at present there is no deep water formation site returning to the high latitude North Atlantic (Fig. 4d) and the freshwater budget shows no signs of a potential recovery. While the subtropical North Atlantic is continuing to increase its salinity, albeit with a very small trend, the subpolar North Atlantic is getting relatively fresher, hampering the restart of deep convection. Also when taking the subpolar North Atlantic and the Arctic into account there is an overall freshening trend suggesting that having a return of deep convection in the high latitude North Atlantic in the near future is very unlikely.

When taking the salinity of the entire Atlantic into account, as was done in Sijp (2012), we do not see a difference in salinity between the hosing and control simulations. In Sijp (2012) the two states in Atlantic mean salinity are associated with the AMOC on and off states. However in Sijp (2012) an RTHC develops, which is responsible for the low salinity state, while in HadGEM3 the AMOC off state still has a shallow wind-driven cell that extends into the Northern Hemisphere, preventing a low salinity state. However if we focus on the region north of 35°N only, the hosing integration is 0.7 psu fresher in the upper 3000 m than the control integration, indicating that low and high salinity states in the subpolar gyre can be associated with the AMOC on and off state in this model. This suggests that a bifurcation in basin average salinity no longer exists in HadGEM3 but bistability in subpolar gyre salinity is still existent.

The increase in northward salt transport by the AMOC in HadGEM3, relative to the coarser resolution climate models (Yin and Stouffer, 2007) is associated with a reduction in vertical gradient of salinity bias in the Atlantic. The model using flux adjustment in Yin and Stouffer (2007), GFDL R30, showed little bias, but the climate model that did not use flux adjustment, GFDL CM2.1, featured larger biases. In particular, the salinity bias in the GFDL CM2.1 model contained a pronounced vertical gradient with a negative salinity bias near the surface and a positive bias at deeper levels throughout most of the Atlantic. Combined with an AMOC that transports surface water northward and deep water southward this salinity bias leads to M_{ov} being strongly biased towards positive values. With a positive M_{ov}, when the AMOC collapses, more saline water will be transported into the Atlantic, aiding the recovery of the AMOC, as is clearly the case with GFDL CM2.1 in Yin and Stouffer (2007). These results are supported by the analysis of Liu et al (2014), where they see a larger negative salinity bias in the surface for the un-flux adjusted models relative to flux adjusted models. This led to a less negative M_{ov} at 34°S, reducing the likelihood of bistability. For the model used in this study, HadGEM3, the salinity bias has a weak negative vertical gradient in the Southern Atlantic in the depths corresponding with the North Atlantic Deep Water (NADW) cell of the AMOC and a mostly positive bias in the upper 1000 m throughout the rest of the Atlantic (Fig. 9). This weaker salinity bias is likely due to the fact that the model is eddy permitting and has swifter and narrower boundary currents. In GFDL CM2.1 the positive salinity bias peaks near 20°N (Yin and Stouffer, 2007), while in HadGEM3 the model bias is smaller there (Fig. 9) since 20°N coincides with a convergence in freshwater transport due to the eddies (Fig. 8e). The vertical structure of the salinity bias in HadGEM3 is too small to affect the sign of M_{ov}: it only has a minor effect on M_{ov} south of the equator and an even weaker effect between the equator and 30°N (Fig. 7). However, a further reduction of the salinity bias would move the model values of M_{ov} even closer to the estimates based on observations of M_{ov} throughout the Atlantic (Fig. 7).

At 26°N M_{ov} is -0.601 Sv in the control integration of HadGEM3 (about -0.6 Sv GFDL CM2.1 Yin and Stouffer (2007)) and -0.78 Sv in observations (McDonagh et al, 2015-in press). A larger difference between HadGEM3 and the models analysed in Yin and Stouffer (2007) occurs at the southern boundary of the subtropical gyre (10°N). In HadGEM3 M_{ov} is largely negative at those latitudes, -0.361 Sv, while in GFDL CM2.1 M_{ov} has about half the amplitude, approximately -0.2 Sv. Both models agree on M_{ov} being slightly negative at the subtropical-subpolar boundary, around -0.2 Sv. Thus the different values at the southern boundary of the subtropical gyre in the models determines the sign of the divergence of M_{ov} over the subtropical gyre and the sign of the advective salt feedback in this area when the AMOC weakens or collapses. Unfortunately there are no estimates of M_{ov} near 10°N, but the reduced salinity bias in HadGEM3 suggests that a negative M_{ov} at those latitudes is the more likely.

Of some concern is the absence of an RTHC in the AMOC streamfunction after hosing is applied. Stability analysis of coarse-resolution ocean-only models suggests that the collapsed AMOC is an unstable steady state, dividing the attractor space between a stable on state and a stable RTHC reaching to the bottom of the Atlantic (Dijkstra, 2007). Furthermore, the studies of Saenko et al (2003) and Sijp et al (2012) point out that it is the density difference between the NADW and the Antarctic Intermediate Water (AAIW) formation regions which are important for the existence of an RTHC. In this study the density of the NADW formation region is not reduced enough after the initial hosing to become lighter than the water in the AAIW formation region as RTHC is not maintained. This study and the results of Yin and Stouffer (2007) suggest that the development of the RTHC is suppressed by atmospheric feedbacks. However, there is at present insufficient analysis to conclude whether atmospheric feedbacks really prevent a stable RTHC to develop, or whether there are other reasons for why it is absent in HadGEM3. For HadGEM3, we believe there are two possibilities; 1) the AMOC off state, despite the maintaining an AMOC off state for much longer than the models used in the PMIP experiment of Stouffer et al (2006), will eventually return to an AMOC on state, or 2) the AMOC off state is a stable solution of coupled climate models at eddy-permitting or higher resolution.

In HadGEM3 the presence of eddies and swifter boundary currents (stronger gyres) allows for stronger northward salt transport of the AMOC, stabilising the off state (Fig. 8). An even higher-resolution (1/12 degree), eddy-resolving ocean model features even larger northward salt transport by M_{eddy} than the eddy-permitting version (Tréguier et al, 2012), implying an AMOC off state could potentially be favoured by even stronger advective salt feedbacks. On the other hand, the latitudinal structure of M_{ov} in HadGEM3 seems broadly consistent with the few estimates we have at different latitudes (Fig. 7) and we anticipate only a small improvement in this respect when going to higher resolution in the ocean component of climate models.

5 Conclusions

The goal of the model run analysed in this study was to rapidly collapse the AMOC and study the stability of the AMOC off state. Several other studies have been done choosing a freshwater hosing setup that more realistically represents what could happen in the climate system (Weijer et al, 2012; Spence et al, 2013; Swingedouw et al, 2013). These studies have all shown that it is possible to weaken the AMOC using a more realistic hosing setup. On top of that Weijer et al (2012) and Spence et al (2013) have shown that when using higher resolution the amount by which the AMOC weakens is larger relative to their coarse resolution models used in those studies. However, these studies often only have been run for 50 years in the high resolution setting. These results plus the results presented in this study support the possibility of coupled models being more likely to model abrupt climate changes as model resolutions continue to improve. At higher resolution a stronger advective salt feedback associated with the AMOC, leading to a freshening of the subtropical North

Atlantic, overcomes the damping feedback that salinifies this region, associated with the atmospheric response to an AMOC collapse. This changed balance between the different feedbacks makes the transition to a stable AMOC off state possible, when the freshwater transports at high latitudes in the North Atlantic increases. This is illustrated by the eddy-permitting climate model, HadGEM3, being able to maintain an AMOC off state for 440 years.

Appendix: Freshwater Budget Calculation

The freshwater budget calculation used in this study is based on the method presented in Drijfhout et al (2011) with modifications to include the effects of a northern and southern boundary, as well as specifics to the version of NEMO used (GO5, version 3.4 of NEMO) (Megann et al, 2013). Mean flow transports are based on 3 month means, while total transports (i.e. vS) are calculated online and are updated after each ocean model time step, which are later averaged over the years of interest removing the effects of the seasonal cycle on the budget. Following Drijfhout et al (2011), the equation for the volume budget is as follows:

$$V_t = T_S - T_N - T_{Med} + PER - Res_V, \tag{2}$$

where V_t is the rate of change of the volume, $T_{(N/S)}$ are volume transports through the northern and southern boundaries, T_{Med} is the volume transport through the Strait of Gibraltar, PER is the precipitation minus evaporation plus runoffs and Res_V is the error generated by the choice of differencing scheme and temporal resolution of the data. The value of Res_V is computed as a residual to close the budget. Since the model has a free surface V_t is equivalent to the changes in the sea surface height using backwards differencing. The main differences between eqn. 2 and eqn. 4 in Drijfhout et al (2011) are that we have left the choice of the northern and southern boundaries as arbitrary as opposed to choosing 34°S and the Bering Strait and we have included a term, T_{med} for the volume transports through the Strait of Gibraltar. In this configuration of NEMO the transports are computed without taking the changes in sea surface height into account. For the regions of interest used in this study the values of Res$_V$ are relatively small resulting in O(10^{-4} Sv) for the North Atlantic subtropical gyre and O(10^{-5} Sv) for the North Atlantic subpolar gyre, which in both cases is the smallest term in the budget with the remaining terms ranging from O(10^{-3} Sv) to O(1 Sv). Choosing instantaneous values of sea surface height from the model restart files in the computation of V_t leads to Res_V having the same order as the precision in which the data is stored but, not all model restart files were available.

Similarly the salinity budget in terms of freshwater becomes the following:

$$M_{trend} - V_t = M_S - M_N - M_{Med} + M_{Mix} - Res_V + H, \tag{3}$$

where M_{trend} is the rate of change of freshwater in the region of interest, $M_{(N/S)}$ are the northward/southward freshwater transports, M_{med} is the freshwater transport through the Strait of Gibraltar, H represents the freshwater hosing and M_{mix}, computed as a residual, closes the budget capturing mixing and errors introduced by the temporal resolution of the data, as well as, the choice of reference salinity, S_o. The conversion between salinity based terms to the freshwater based terms in eqn. 3 is done through multiplying all the terms in the equation by $-1/S_o$. Note that we have dropped the negative sign before M_{trend} in eqn. 3, contrary to Drijfhout et al (2011) so that positive values indicate an increase in freshwater not salinity. In this case the hosing is included in the salinity budget and not the volume budget since it is computed as a redistribution of salinity in this model study. Combining eqns. 2 and 3 gives the following expression for the fresh water budget:

$$M_{trend} = (M_S + T_S) - (M_N + T_N) - (M_{Med} + T_{Med}) + M_{Mix} + PER + H. \tag{4}$$

The $M_{(N/S)}$ terms can be divided into eddy and mean flow components since the ocean model output includes vS computed at every model time step. The eddy contribution to the freshwater transport is defined as follows:

$$M_{(eddy(N/S))} = \frac{-1}{S_o} \int_{N/S} (\overline{vS} - \overline{v}\overline{S}) dA = M_{(N/S)} - M_{(mean(N/S))}, \tag{5}$$

$$\rightarrow M_{(N/S)} = M_{(mean(N/S))} + M_{(eddy(N/S))}, \tag{6}$$

where the integral is taken over each zonal section of the Atlantic basin, $\overline{vS}$ is the total seasonal mean transport, $\overline{v}$ and $\overline{S}$ are the seasonal mean meridional velocity and salinity and $M_{(mean(S/N))} = -1/S_o \int_{N/S} \overline{v}\,\overline{S} dA$ represents the non-eddy transports, with the overbar denoting a mean computed over 3 months. A map of the eddy kinetic energy (Fig. 10) shows that the eddy field in HadGEM3 is very similar to other models of similar resolution (Delworth et al, 2012), perhaps even slightly closer to what is expected from observations. The eddy contribution is computed in a very similar way to Tréguier et al (2012), in which it was also shown that the eddy contribution will be even stronger at higher model resolutions. Since the current model resolution is eddy-permitting it is not possible to completely resolve eddies at all latitudes, therefore caution must be taken in interpreting the role of the eddies in the high latitudes. Similar to what is done in Drijfhout et al (2011), $M_{(mean(S/N))}$ can be divided into an overturning $M_{(ov(S/N))}$, azonal $M_{(az(S/N))}$ and the volume transport $T_{(S/N)}$ terms as follows:

$$M_{mean(N/S)} = M_{ov(N/S)} + M_{az(N/S)} - T_{(N/S)}, \tag{7}$$

$$M_{ov(N/S)} = \frac{-1}{S_o} \int_{N/S} v^* \langle S \rangle dA, \tag{8}$$

$$M_{az(N/S)} = \frac{-1}{S_o} \int_{N/S} v' S' dA, \tag{9}$$

where $\langle f \rangle = \int f dx / \int x$ is the zonal mean, $f' = f - \langle f \rangle$ is the difference from the zonal mean, $\hat{f} = \int f dA / \int dA$ is the zonal section mean or barotropic component and $f^* = \langle f \rangle - \hat{f}$ is the zonal mean baroclinic component for $f = \overline{v}$ or $f = \overline{S}$. Substituting eqns. 6 and 7 into eqn. 4 gives the final form for the zonal freshwater budget equation:

$$M_{trend} = \Delta M_{ov} + \Delta M_{az} + \Delta M_{eddy} + \Delta M_{Med} + M_{Mix} + PER + H, \tag{10}$$

where $\Delta M_{ov} = M_{(ov(S))} - M_{(ov(N))}$, $\Delta M_{az} = M_{(az(S))} - M_{az(N)}$, $\Delta M_{eddy} = M_{(eddy(S))} - M_{(eddy(N))}$ and $\Delta M_{Med} = -M_{Med} - T_{Med}$.

The are several possible valid choices of the reference salinity; the mean salinity over the entire volume of the region used in the budget calculation, the mean salinity over the section used as the northern (southern) boundary or the mean salinity from the Strait of Gibraltar. For this study it was chosen to use the mean salinity at the boundary between the North Atlantic subtropical and subpolar gyres for S_o, the reference salinity. Choosing one of the other salinities as a reference salinity creates a maximum difference of O(10-4 Sv), which is less than 10% of the smallest value represented in our budget analysis. To further simplify the budget analysis only times when there is no hosing being applied are considered and the freshwater transport through the Strait of Gibraltar is combined with the mixing term, resulting in the following final equation for the budget analysis:

$$M_{trend} = \Delta M_{ov} + \Delta M_{az} + \Delta M_{eddy} + M_{mix} + PER. \tag{11}$$

Acknowledgements We acknowledge use of the MONSooN system, a collaborative facility supplied under the Joint Weather and Climate Research Programme, a strategic partnership between the UK Met Office and the Natural Environment Research Council. We would also like to thank Matt Mizlienski for helping setup the model as well as, Jeff Blundell and Adam Blaker for technical support. Finally we wish to thank two anonymous reviewers for their comments which improved this manuscript.

References

de Abreu L, Shackleton NJ, Schönfeld J, Hall M, Chapman M (2003) Millennial-scale oceanic climate variability off the Western Iberian margin during the last two glacial periods. Marine Geology 196(1):1–20, DOI 10.1016/S0025-3227(03)00046-X

Blunier T, Brook EJ (2001) Timing of millennial-scale climate change in Antarctica and Greenland during the last glacial period. Science 291(5501):109–112, DOI 10.1126/science.291.5501.109

de Boyer Montégut C, Madec G, Fischer AS, Lazar A, Iudicone D (2004) Mixed layer depth over the global ocean: An examination of profile data and a profile-based climatology. Journal of Geophysical Research: Oceans (1978–2012) 109(C12), DOI 10.1029/2004JC002378

Broecker WS, Bond G, Klas M, Bonani G, Wolfli W (1990) A salt oscillator in the glacial Atlantic? 1. The concept. Paleoceanography 5(4):469–477

Bryden HL, King BA, McCarthy GD (2011) South Atlantic overturning circulation at 24 S. Journal of Marine Research 69(1):38–55, DOI 10.1357/002224011798147633

Collins M, Knutti R, Arblaster J, Dufresne JL, Fichefet T, Friedlingstein P, Gao X, Gutowski W, Johns T, Krinner G, et al (2013) Long-term climate change: projections, commitments and irreversibility

Danabasoglu G, Yeager SG, Bailey D, Behrens E, Bentsen M, Bi D, Biastoch A, Böning C, Bozec A, Canuto VM, et al (2014) North Atlantic simulations in coordinated ocean-ice reference experiments phase II (CORE-II). Part I: mean states. Ocean Modelling 73:76–107, DOI 10.1016/j.ocemod.2013.10.005

Dansgaard W, Johnsen S, Clausen H, Dahl-Jensen D, Gundestrup N, Hammer C, Hvidberg C, Steffensen J, Sveinbjörnsdottir A, Jouzel J, et al (1993) Evidence for general instability of past climate from a 250-kyr ice-core record. Nature 364(6434):218–220, DOI 10.1038/364218a0

Delworth TL, Rosati A, Anderson W, Adcroft AJ, Balaji V, Benson R, Dixon K, Griffies SM, Lee HC, Pacanowski RC, et al (2012) Simulated climate and climate change in the gfdl cm2. 5 high-resolution coupled climate model. Journal of Climate 25(8):2755–2781, DOI 10.1175/JCLI-D-11-00316.1

Dijkstra HA (2007) Characterization of the multiple equilibria regime in a global ocean model. Tellus A 59(5):695–705, DOI 10.1111/j.1600-0870.2007.00267.x

Drijfhout SS (2010) The atmospheric response to a thermohaline circulation collapse: scaling relations for the hadley circulation and the response in a coupled climate model. Journal of Climate 23(3):757–774, DOI 10.1175/2009JCLI3159.1

Drijfhout SS (2014) Global radiative adjustment after a collapse of the Atlantic meridional overturning circulation. Climate Dynamics pp 1–11, DOI 10.1007/s00382-014-2433-9

Drijfhout SS, Weber SL, van der Swaluw E (2011) The stability of the MOC as diagnosed from model projections for pre-industrial, present and future climates. Climate dynamics 37(7-8):1575–1586, DOI 10.1007/s00382-010-0930-z

Garzoli SL, Baringer MO, Dong S, Perez RC, Yao Q (2013) South Atlantic meridional fluxes. Deep Sea Research Part I: Oceanographic Research Papers 71:21–32, DOI 10.1016/j.dsr.2012.09.003

Hansen B, Østerhus S (2007) Faroe bank channel overflow 1995–2005. Progress in Oceanography 75(4):817–856, DOI 10.1016/j.pocean.2007.09.004

Hawkins E, Smith RS, Allison LC, Gregory JM, Woollings TJ, Pohlmann H, de Cuevas B (2011) Bistability of the Atlantic overturning circulation in a global climate model and links to ocean freshwater transport. Geophysical Research Letters 38(10), DOI 10.1029/2011GL047208

Hewitt H, Copsey D, Culverwell I, Harris C, Hill R, Keen A, McLaren A, Hunke E (2011) Design and implementation of the infrastructure of HadGEM3: The next-generation Met Office climate modelling system. Geoscientific Model Development 4(2):223–253, DOI doi:10.5194/gmd-4-223-2011

Hu A, Meehl GA, Han W, Timmermann A, Otto-Bliesner B, Liu Z, Washington WM, Large W, Abe-Ouchi A, Kimoto M, et al (2012) Role of the Bering Strait on the hysteresis of the ocean conveyor belt circulation and glacial climate stability. Proceedings of the National Academy of Sciences 109(17):6417–6422, DOI 10.1073/pnas.1116014109

Huisman SE, Den Toom M, Dijkstra HA, Drijfhout S (2010) An indicator of the multiple equilibria regime of the Atlantic meridional overturning circulation. Journal of physical oceanography 40(3):551–567, DOI 10.1175/2009JPO4215.1

Ingleby B, Huddleston M (2007) Quality control of ocean temperature and salinity profiles: Historical and real-time data. Journal of Marine Systems 65(1):158–175, DOI 10.1016/j.jmarsys.2005.11.019

Jackson L (2013) Shutdown and recovery of the AMOC in a coupled global climate model: the role of the advective feedback. Geophysical Research Letters 40(6):1182–1188, DOI 10.1002/grl.50289

Jackson L, Kahana R, Graham T, Ringer M, Woollings T, Mecking J, Wood R (2015) Global and European climate impacts of a slowdown of the AMOC in a high resolution GCM. Climate Dynamics pp 1–18, DOI 10.1007/s00382-015-2540-2

Jochumsen K, Quadfasel D, Valdimarsson H, Jonsson S (2012) Variability of the Denmark Strait overflow: Moored time series from 1996–2011. Journal of Geophysical Research: Oceans (1978–2012) 117(C12), DOI 10.1029/2012JC008244

Kanzow T, Cunningham S, Johns W, Hirschi JJ, Marotzke J, Baringer M, Meinen C, Chidichimo M, Atkinson C, Beal L, et al (2010) Seasonal variability of the Atlantic meridional overturning circulation at 26.5 N. Journal of Climate 23(21):5678–5698, DOI 10.1175/2010JCLI3389.1

Krebs U, Timmermann A (2007) Tropical air-sea interactions accelerate the recovery of the Atlantic meridional overturning circulation after a major shutdown. Journal of Climate 20(19):4940–4956, DOI 10.1175/JCLI4296.1

Liu W, Liu Z (2013) A diagnostic indicator of the stability of the Atlantic meridional overturning circulation in CCSM3. Journal of Climate 26(6):1926–1938, DOI 10.1175/JCLI-D-11-00681.1

Liu W, Liu Z, Brady EC (2014) Why is the AMOC Monostable in Coupled General Circulation Models? Journal of Climate 27(6):2427–2443, DOI 10.1175/JCLI-D-13-00264.1

Madec G (2008) NEMO ocean engine

Manabe S, Stouffer R (1988) Two stable equilibria of a coupled ocean-atmosphere model. Journal of Climate 1(9):841–866, DOI 10.1175/1520-0442(1988)001<0841:TSEOAC>2.0.CO;2

Marotzke J (1990) Instabilities and multiple equilibria of the thermohaline circulation. PhD thesis, Christian-Albrechts-Universität

McDonagh EL, King BA (2005) Oceanic fluxes in the South Atlantic. Journal of physical oceanography 35(1):109–122, DOI 10.1175/JPO-2666.1

McDonagh EL, McLeod P, King BA, Bryden HL, Valdés ST (2010) Circulation, heat, and freshwater transport at 36 N in the Atlantic. Journal of Physical Oceanography 40(12):2661–2678, DOI 10.1175/2010JPO4176.1

McDonagh EL, King BA, Bryden HL, Courtois P, Szuts Z, Baringer M, Cunningham S, Atkinson C, McCarthy G (2015-in press) Continuous estimate of Atlantic oceanic freshwater flux at 26.5°N. Journal of Climate

Megann A, Storkey D, Aksenov Y, Alderson S, Calvert D, Graham T, Hyder P, Siddorn J, Sinha B (2013) GO5. 0: The joint NERC-Met Office NEMO global ocean model for use in coupled and forced applications. Geoscientific Model Development Discussions 6(4):5747–5799, DOI 10.5194/gmdd-6-5747-2013

Peltier W, Vettoretti G, Stastna M (2006) Atlantic meridional overturning and climate response to Arctic Ocean freshening. Geophysical Research Letters 33(6), DOI 10.1029/2005GL025251

Rae J, Hewitt H, Keen A, Ridley J, West A, Harris C, Hunke E, Walters D (2015) Development of Global Sea Ice 6.0 CICE configuration for the Met Office Global Coupled Model. Geoscientific Model Development Discussions 8(3):2529–2554, DOI 10.5194/gmdd-8-2529-2015

Rahmstorf S (1996) On the freshwater forcing and transport of the Atlantic thermohaline circulation. Climate Dynamics 12(12):799–811, DOI 10.1007/s003820050144

Saenko OA, Weaver AJ, Gregory JM (2003) On the link between the two modes of the ocean thermohaline circulation and the formation of global-scale water masses. Journal of climate 16(17):2797–2801, DOI 10.1175/1520-0442(2003)016<2797:OTLBTT>2.0.CO;2

Scaife A, Arribas A, Blockley E, Brookshaw A, Clark R, Dunstone N, Eade R, Fereday D, Folland C, Gordon M, et al (2014) Skillful long-range prediction of European and North American winters. Geophysical Research Letters 41(7):2514–2519, DOI 10.1002/2014GL059637

Scaife AA, Copsey D, Gordon C, Harris C, Hinton T, Keeley S, O'Neill A, Roberts M, Williams K (2011) Improved Atlantic winter blocking in a climate model. Geophysical Research Letters 38(23), DOI 10.1029/2011GL049573

Sijp WP (2012) Characterising meridional overturning bistability using a minimal set of state variables. Climate dynamics 39(9-10):2127–2142, DOI 10.1007/s00382-011-1249-0

Sijp WP, England MH, Gregory JM (2012) Precise calculations of the existence of multiple AMOC equilibria in coupled climate models. Part I: Equilibrium states. Journal of Climate 25(1):282–298, DOI 10.1175/2011JCLI4245.1

Smeed D, McCarthy G, Cunningham S, Frajka-Williams E, Rayner D, Johns W, Meinen C, Baringer M, Moat B, Duchez A, et al (2014) Observed decline of the Atlantic meridional overturning circulation 2004–2012. Ocean Science 10(1):29–38, DOI 10.5194/os-10-29-2014

Spence P, Saenko OA, Sijp W, England MH (2013) North Atlantic climate response to Lake Agassiz drainage at coarse and ocean eddy-permitting resolutions. Journal of Climate 26(8):2651–2667, DOI 10.1175/JCLI-D-11-00683.1

Stommel H (1961) Thermohaline convection with two stable regimes of flow. Tellus 13(2):224–230

Stouffer RJ, Yin J, Gregory J, Dixon K, Spelman M, Hurlin W, Weaver A, Eby M, Flato G, Hasumi H, et al (2006) Investigating the causes of the response of the thermohaline circulation to past and future climate changes. Journal of Climate 19(8):1365–1387, DOI 10.1175/JCLI3689.1

Swingedouw D, Rodehacke CB, Behrens E, Menary M, Olsen SM, Gao Y, Mikolajewicz U, Mignot J, Biastoch A (2013) Decadal fingerprints of freshwater discharge around Greenland in a multi-model ensemble. Climate dynamics 41(3-4):695–720, DOI 10.1007/s00382-012-1479-9

Tréguier AM, Theetten S, Chassignet EP, Penduff T, Smith R, Talley L, Beismann J, Böning C (2005) The North Atlantic subpolar gyre in four high-resolution models. Journal of Physical Oceanography 35(5):757–774, DOI 10.1175/JPO2720.1

Tréguier AM, Deshayes J, Lique C, Dussin R, Molines JM (2012) Eddy contributions to the meridional transport of salt in the North Atlantic. Journal of Geophysical Research: Oceans (1978–2012) 117(C5), DOI 10.1029/2012JC007927

Valdes P (2011) Built for stability. Nature Geoscience 4(7):414–416

Vellinga M, Wood RA (2002) Global climatic impacts of a collapse of the Atlantic thermohaline circulation. Climatic change 54(3):251–267, DOI 10.1023/A:1016168827653 de Vries P, Weber SL (2005) The Atlantic freshwater budget as a diagnostic for the existence of a stable shut down of the meridional overturning circulation. Geophysical research letters 32(9), DOI 10.1029/2004GL021450

Weijer W, Maltrud M, Hecht M, Dijkstra H, Kliphuis M (2012) Response of the Atlantic Ocean circulation to Greenland Ice Sheet melting in a strongly-eddying ocean model. Geophysical Research Letters 39(9), DOI 10.1029/2012GL051611

Williams K, Harris C, Bodas-Salcedo A, Camp J, Comer R, Copsey D, Fereday D, Graham T, Hill R, Hinton T, Hyder P, Ineson S, Masato G, Milton S, Roberts M, Rowell D, Sanchez C, Shelly A, Sinha B, Walters D, West A, Woollings T, Xavier P (2015) The Met Office Global Coupled model 2.0 (GC2) configuration. Geoscientific Model Development 8:1509–1524, DOI 10.5194/gmd-8-1509-2015

Wunsch C (2002) What is the thermohaline circulation. Science 298(5596):1179–1181, DOI 10.1126/science.1079329

Wunsch C (2006) Abrupt climate change: An alternative view. Quaternary Research 65(2):191–203, DOI 10.1016/j.yqres.2005.10.006

Yin J, Stouffer RJ (2007) Comparison of the stability of the Atlantic thermohaline circulation in two coupled atmosphere-ocean general circulation models. Journal of Climate 20(17):4293–4315, DOI 10.1175/JCLI4256.1

Table 1 Summary of freshwater budget for subtropical (10°N-45°N) and subpolar North Atlantic (45°N-70°N). All values are given in Sv with positive values indicating an addition of freshwater into the region. The bottom row of each section is the anomalous change in freshwater (i.e. Hosing (311-410) - Control).

		Overturning ΔM_{ov}	**Azonal** ΔM_{az}	**Eddy** ΔM_{eddy}	**P-E+R** PER	**Mixing** M_{mix}	**Total** M_{trend}
Subpolar N. Atlantic	Control	-0.170	-0.090	-0.033	0.241	0.041	-0.012
	Hosing (311-410)	-0.165	-0.187	-0.031	0.283	0.093	-0.007
	Anomaly	0.006	-0.097	0.001	0.042	0.052	0.005
Subtropical N. Atlantic	Control	-0.164	0.524	0.102	-0.504	-0.009	-0.051
	Hosing (311-410)	-0.032	0.490	0.061	-0.551	-0.024	-0.055
	Anomaly	0.132	-0.033	-0.041	-0.047	-0.015	-0.004

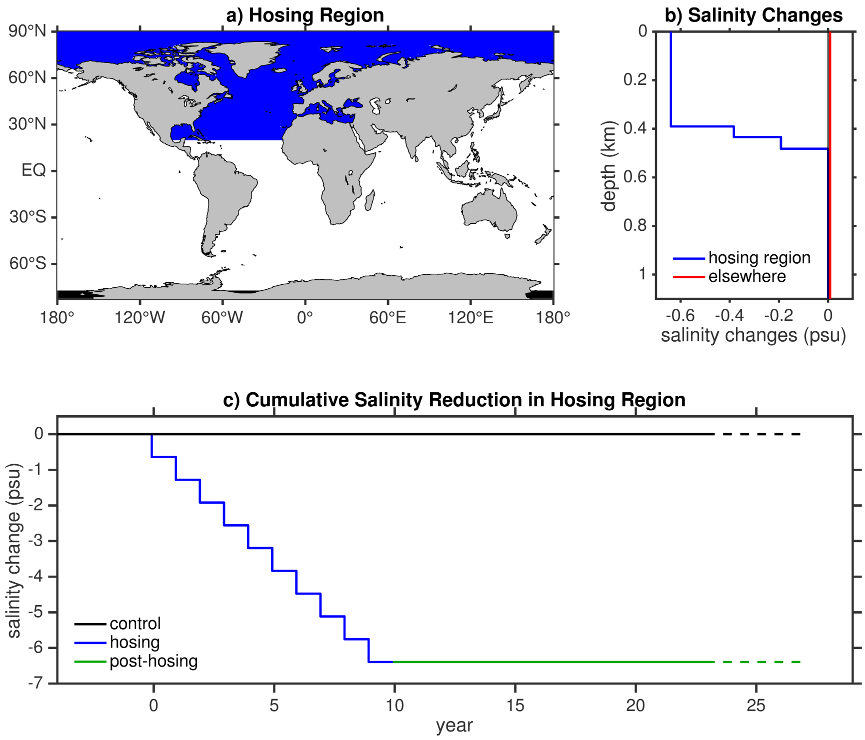

Fig. 1 (a) The region where the freshwater hosing is applied. (b) The redistribution of salinity in the hosing region (blue) and everywhere else (red). (c) The cumulative salinity reduction in the hosing region (upper 350 m) in the model experiments for the control (black), hosing (blue) post-hosing (green).

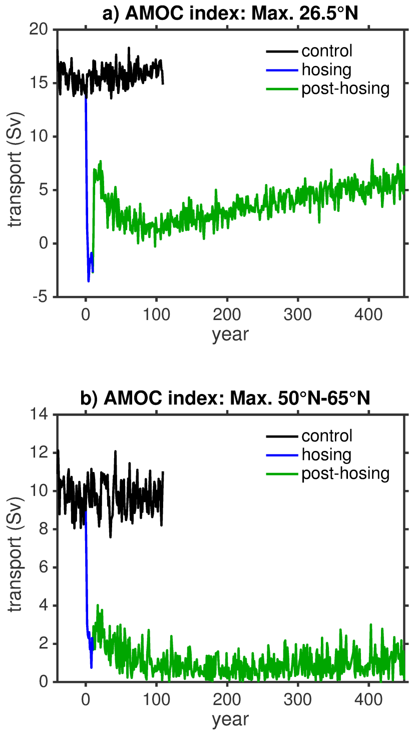

Fig. 2 (a) The AMOC index computed as the maximum AMOC streamfunction at 26.5°N below a depth of 500 m and above 2000 m for the control experiment (black), hosing period (blue) and post-hosing period (green). (b) same as a expect computed between 50°N and 65°N.

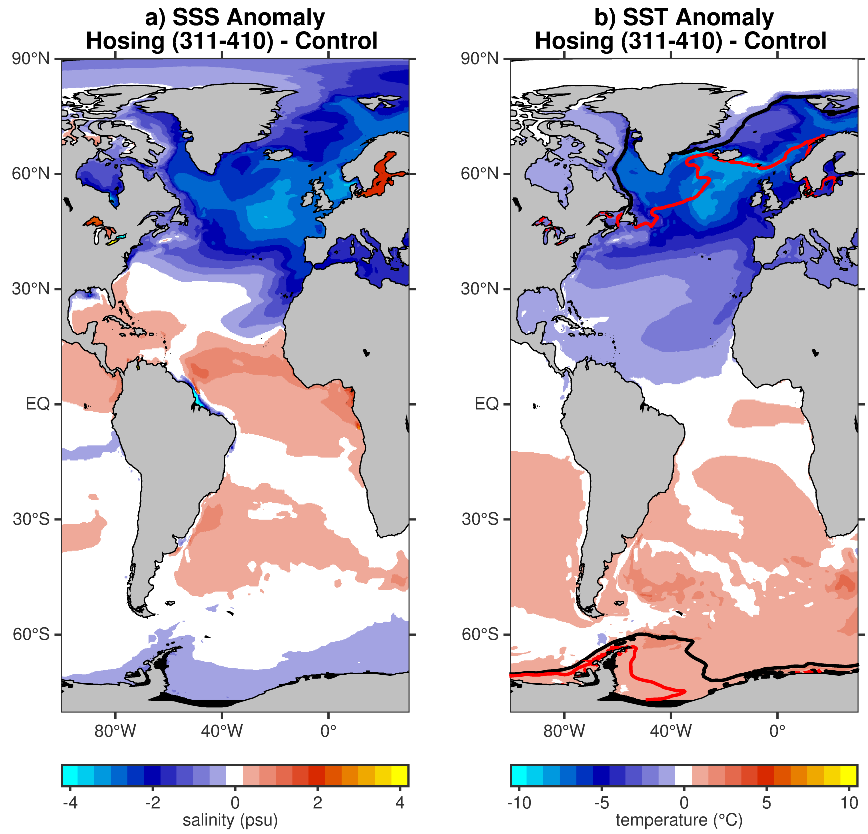

Fig. 3 (a) Mean SSS from years 311-410 of the hosing simulation minus the mean SSS from the control simulation. (b) same as in (a) but for SST with the black contour indicating the annual maximum sea-ice extent in the control simulation and the red contour from years 311-410 of the hosing simulation.

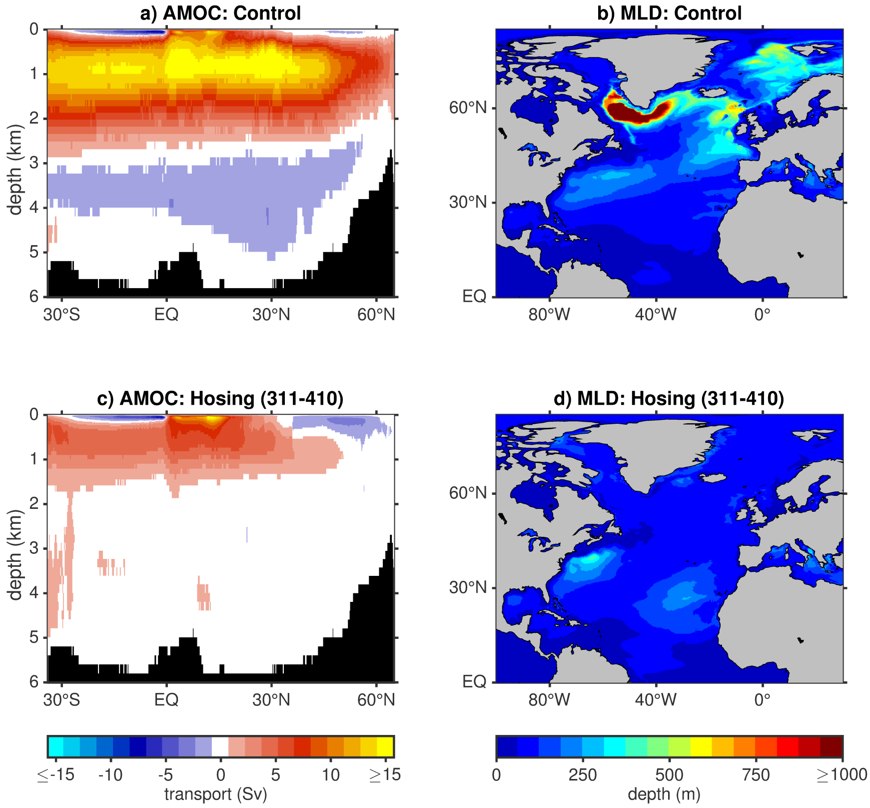

Fig. 4 (a) The mean AMOC streamfunction and (b) the mean annual maximum mixed layer depth from the control simulation. (c) and (d) same as a and b but for years 311-410 of the hosing simulation.

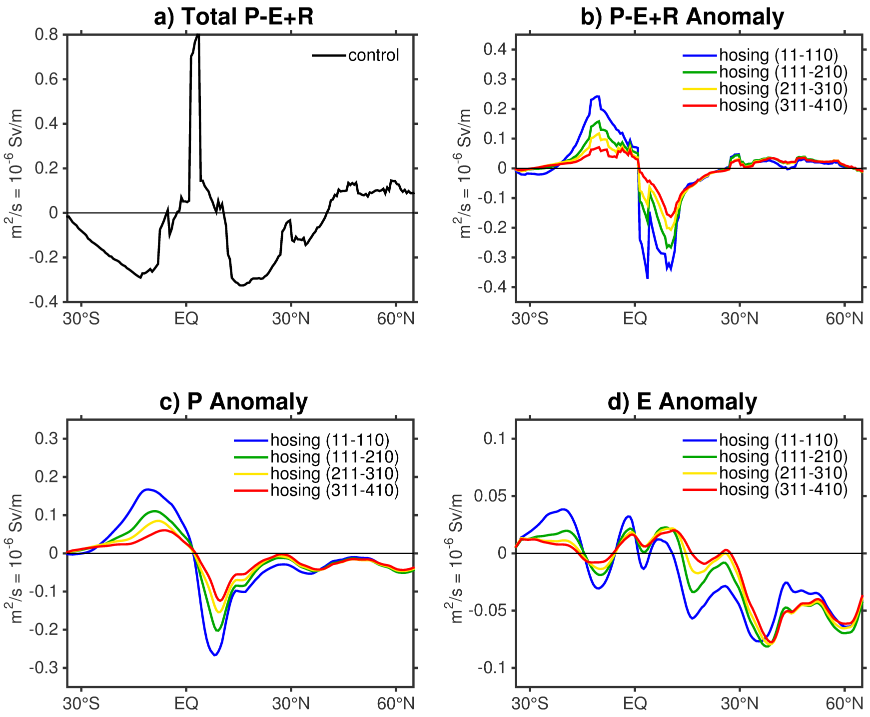

Fig. 5 (a) The zonally integrated P-E+R from the control simulation normalized to Sv per meter in latitude. (b) the anomalous P-E+R from various 100 year means in the hosing simulation, (c) same as b but for precipitation only, (d) same as b but for evaporation only with blue years 11-110, green years 111-210 yellow years 211-310 and red years 311-410. All data is smoothed using at 2° latitude window to reduce the spikes from the river runoffs.

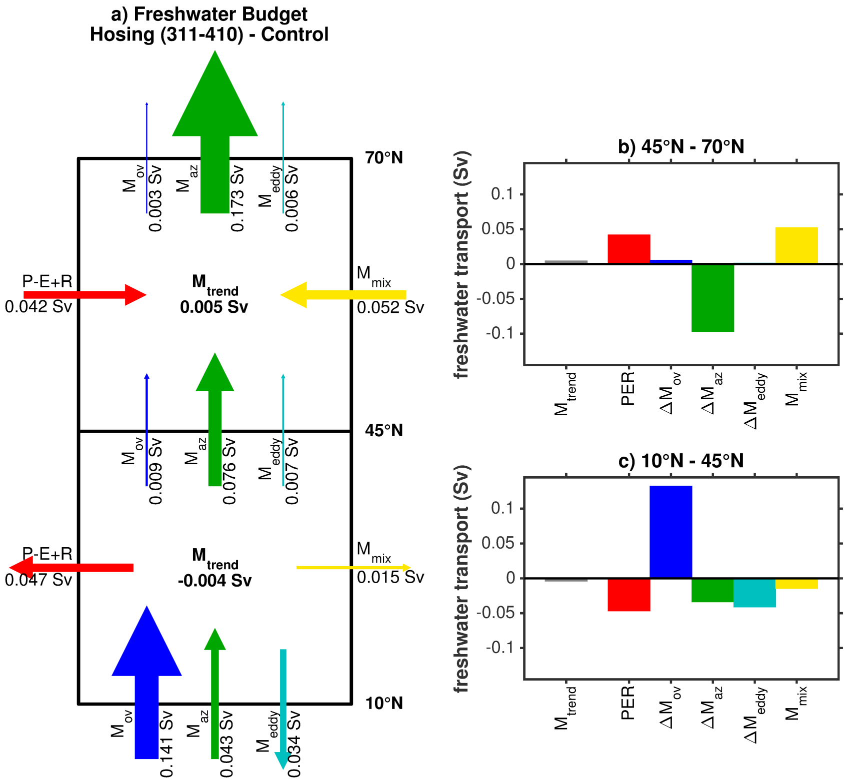

Fig. 6 (a) Anomalous freshwater budget boxes for the subtropical (10°N-45°N) and subpolar (45°N-70°N) North Atlantic. The width of the arrows and arrow heads have been scaled according to the strength of the freshwater transport anomalies. (b) Summary of the anomalous freshwater budget for the subpolar North Atlantic. (c) Same as (b) but for the subtropical North Atlantic.

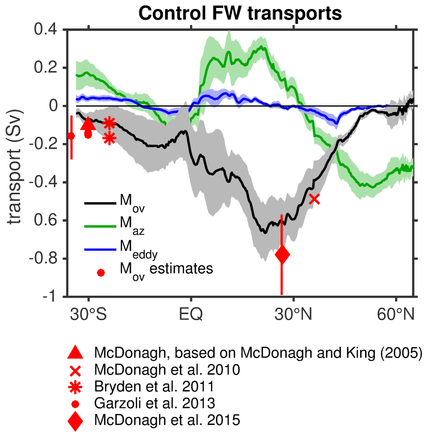

Fig. 7 Mean M_{ov} from control simulation with $\pm$ one standard deviation of seasonal data (black/grey shading), mean M_{az} from control simulation with $\pm$ one standard deviation of seasonal data (green/green shading) and mean M_{eddy} from control simulation with $\pm$ one standard deviation of seasonal data (blue/blue shading). Estimates of M_{ov} from observations (red): triangle based on McDonagh and King (2005); cross McDonagh et al (2010); stars Bryden et al (2011); circles Garzoli et al (2013) with vertical line representing the range in estimates; and diamond McDonagh et al (2015-in press) with the vertical line indicating the standard deviation of 10 day timeseries. Note that the standard deviations/range are computed using data available on different timescales.

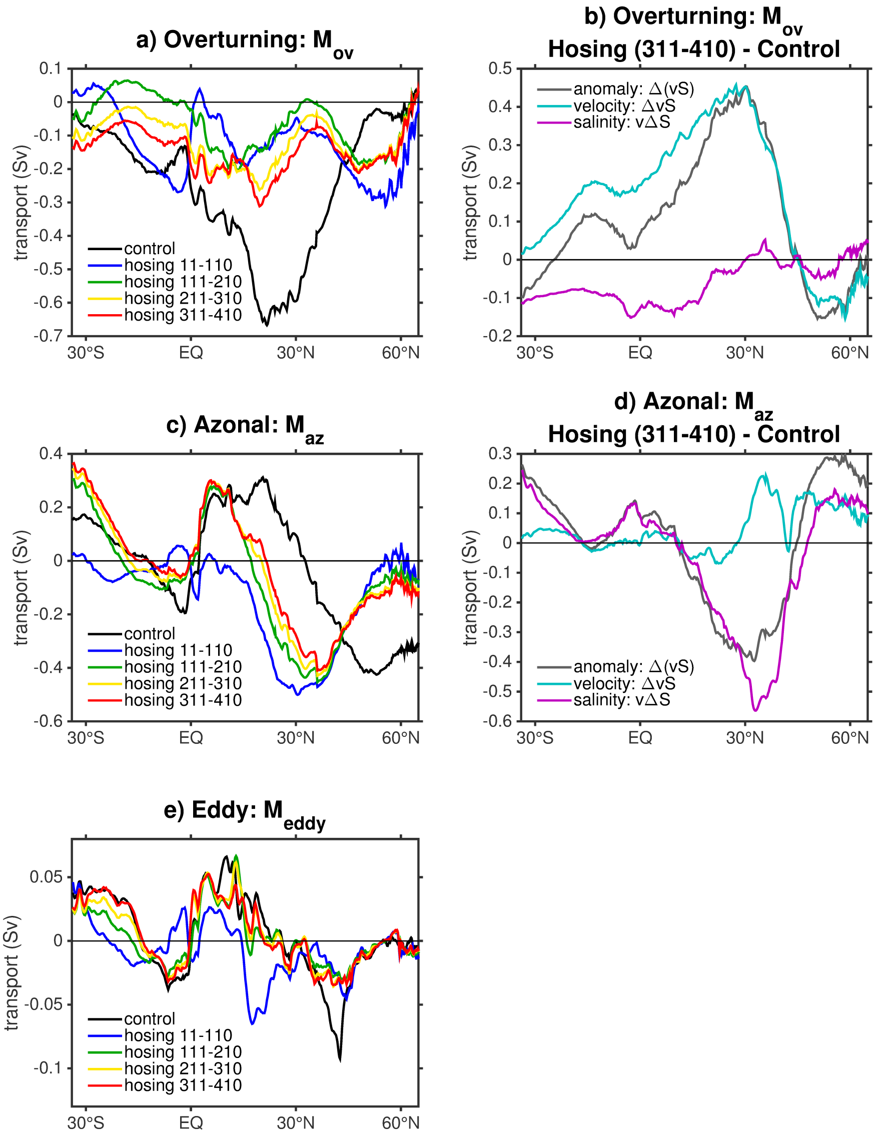

Fig. 8 The freshwater transports along latitude bands in the Atlantic. (a) Freshwater transport due overturning M_{ov}. The different colours represent different means over various years; control (black), hosing 11-110 (blue), hosing 111-210 (green), hosing 211-310 (yellow) and hosing 311-410 (red). (b) Decomposition of M_{ov} anomalies (hosing years 311-410 minus control) into contributions from velocity (cyan) and salinity (magenta) compared to total anomaly (dark gray). (c and d) same as (a and b) but for M_{az} and (e) same as (a) but for M_{eddy}. Note the different scales on panels a-e.

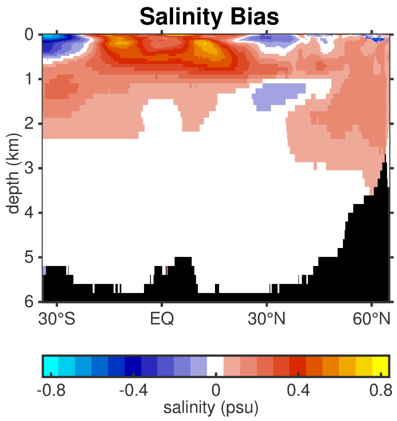

Fig. 9 Zonal mean salinity bias of the control experiment relative to EN3 data (Ingleby and Huddleston, 2007).

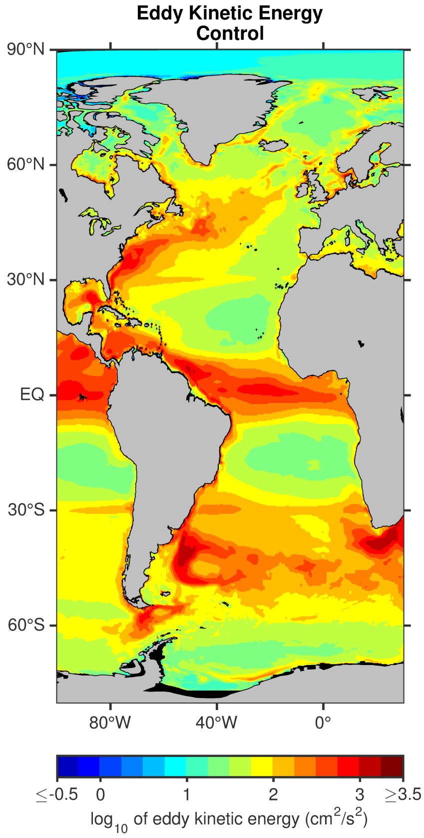

Fig. 10 Logarithm of the surface eddy kinetic energy in the control simulation. The eddy kinetic energy was computed from the model's surface velocity fields using the difference between the instantaneous velocities and seasonal mean velocities before averaging over all years of the simulation.